Femtosecond valley polarization and topological resonances in transition metal dichalcogenides

S. Azar Oliaei Motlagh, Jhih-Sheng Wu, Vadym Apalkov, and Mark I. Stockman

Phys. Rev. B **98**, 081406 — Published 15 August 2018

DOI: 10.1103/PhysRevB.98.081406

Femtosecond valley polarization and topological resonances in transition metal dichalcogenides

S. Azar Oliaei Motlagh, Jhih-Sheng Wu, Vadym Apalkov, and Mark I. Stockman
Center for Nano-Optics (CeNO) and Department of Physics and Astronomy, Georgia State University, Atlanta, Georgia 30303, USA
(Dated: August 6, 2018)

We theoretically introduce the fundamentally fastest induction of a significant population and valley polarization in a monolayer of a transition metal dichalcogenide (i.e., MoS_2 and WS_2). This may be extended to other two-dimensional materials with the same symmetry. This valley polarization can be written and read-out by a pulse consisting of just a single optical oscillation with a duration of a few femtoseconds and an amplitude of ~ 0.25 V/Å. Under these conditions, we predict a new effect of *topological resonance*, which is due to Bloch motion of electrons in the reciprocal space where electron population textures are formed due to non-Abelian Berry curvature. The predicted phenomena can be applied for information storage and processing in PHz-band optoelectronics.

Femtosecond and attosecond technology has made it possible to control and study ultrafast electron dynamics in three-dimensional solids[1–6]. There is a wide class of two-dimensional (2D) crystals, which have unique and useful properties[7–14] that bear a promise for applications in ultrafast opto-electronics[15]. However, not all 2D materials are suitable for any given application. For example, graphene is a well-studied 2D material, which is semimetallic with no bandgap between the valence band (VB) and the conduction band (CB). This causes a relatively high off-current in graphene transistors drastically limiting their usefulness[16–19]. In contrast, there is a broad class of 2D semiconductors possessing finite direct bandgaps. Among them, transition metal dichalcogenides (TMDC's) possess direct bandgaps of $1.1-2.1$ eV[7,10,11,20–22].

Similar to graphene, TMDC monolayers have hexagonal lattices constituted by two triangular sublattices[10,18,20]. Unlike graphene, these sublattices consist of different atoms (metal and chalcogen), which breaks the inversion ($\mathcal{P}$) symmetry and opens up bandgaps at the K, K'-points whose degeneracy is protected by time reversal ($\mathcal{T}$) symmetry[18,23].

The $\mathcal{T}$-symmetry and K, K'-valley degeneracy can be relaxed by circularly-polarized optical pumping, which allows for a highly valley-specific electron population, depending on the helicity of the excitation pulse[21,23–27]. This selective valley population, known as valley polarization, introduces a new area referred to as valleytronics[12,28]. A significant spin-orbit coupling (SOC) makes these materials promising also for spintronics[21,25].

In this article, we theoretically introduce the fundamentally fastest induction of significant population and valley polarization in MoS_2 and WS_2 monolayers by a *single* cycle of a strong circularly-polarized optical field with duration of a few femtoseconds and amplitude of $0.2-0.5$ VÅ^{-1}. This process is determined by electron motion in the reciprocal space, spanning a significant part of the Brillouin zone. This motion also causes a new effect, *topological resonance*, which we introduce below in discussion of Fig. 1.

For a single-oscillation pulse, optical electric field $\mathbf{F}(t)$ as a function of time t is parametrized as

$$F_x(t) = F_0(1-2u^2)e^{-u^2}\ , \quad F_y(t) = \pm 2uF_0e^{-u^2}\ , \quad (1)$$

where $u = t/\tau$, and $\tau = 1$ fs determines the pulse duration and its mean frequency [see Supplemental Materials (SM) for definition] $\hbar\bar{\omega} \approx 1.2$ eV. The $\pm$ sign defines helicity of the applied pulse: $+$ for the right-handed and $-$ for the left-handed circular polarization. These left- and right-handed pulses are mutually $\mathcal{T}$-reversed. A few- or single-oscillation pulses are presently experimentally available from near-ultraviolet through terahertz range in linear[29–35] or circularly polarization[34,36].

We set the TMDC monolayer in the xy plane with the pulse incident in the z direction. We use a three-band tight binding (TB) (third nearest neighbor) model Hamiltonian[20], $H^{\rm TNN}$, see Eq. (1) of SM. The TB Hamiltonian of a TMDC monolayer is constituted by three orbitals, d_{z^2}, d_{xy}, and $d_{x^2-y^2}$ of the metal atom. The full Hamiltonian is $H(t) = H^{\rm TNN} + H^{\rm SOC} + H^{\rm int}(t)$, where $H^{\rm SOC}$ is the SOC term [Eq. (3) of SM], and $H^{\rm int}(t)$ is the light-TMDC interaction term. In the length gauge $H^{\rm int} = -e\mathbf{F}(t)\mathbf{r}$, where e is electron charge. This model includes three bands: valence band (VB) and two conduction bands (CB's), each band spin-split into two bands.

We assume that electron collisions can be neglected because the applied pulse (a few femtoseconds) is much shorter than the electron scattering (dephasing) time in TMDC's. In fact, this dephasing time was 500 fs for an atomically thin MoS_2[37]. Also, Ref. 38 reported electron coherence times for WSe_2 to be 150 fs to 410 fs. In Ref. 39, the dephasing time was calculated to be ≈ 37 fs for a few layers of MoS_2. Carrier relaxation time in MoS_2 was found to be 25 ps, and the electron-hole recombination time to be 300 ps[40]. Based on this, we describe the electron dynamics as coherent by time-dependent Schrödinger equation (TDSE). Previously, such a TDSE theory[41–49] was successful in predicting new effects and describing expermental results in both three-dimensional solids[2,3,50] and graphene[51]. For non-interacting particles,

the TDSE theory is fundamentally equivalent to the density matrix equations but is computationally much more efficient.

In solids, an applied electric field generates both intraband and interband electron dynamics. The intraband dynamics is determined by the Bloch acceleration theorem[52]: for an electron with an initial crystal momentum $\mathbf{q}$, time-dependent crystal momentum $\mathbf{k}(\mathbf{q},t)$ is

$$\mathbf{k}(\mathbf{q},t) = \mathbf{q} + \frac{e}{\hbar}\int_{-\infty}^{t} \mathbf{F}(t')dt'. \tag{2}$$

The corresponding wave functions, which are solutions of the TDSE,

$$i\hbar\frac{d\Psi}{dt} = H(t)\Psi \ , \tag{3}$$

within a single band α, are the well-known Houston functions[53],

$$\Phi^{(H)}_{\alpha\mathbf{q}}(\mathbf{r},t) = \Psi^{(\alpha)}_{\mathbf{k}(\mathbf{q},t)}(\mathbf{r})e^{-\frac{i}{\hbar}\int_{-\infty}^{t} dt_1 E_\alpha[\mathbf{k}(\mathbf{q},t_1)]} \ , \tag{4}$$

where $\alpha = v, c_1, c_2$ for the VB and CB's, correspondingly, $\Psi^{(\alpha)}_{\mathbf{k}}$ are Bloch-band eigenfunctions in the absence of the pulse field, and $E_\alpha(\mathbf{k})$ is the band energy.

The interband electron dynamics is determined by the solution, $\Psi_{\mathbf{q}}(\mathbf{r},t)$, of TDSE (3), which can be expressed in the basis of the Houston functions $\Phi^{(H)}_{\alpha\mathbf{q}}(\mathbf{r},t)$,

$$\Psi_{\mathbf{q}}(\mathbf{r},t) = \sum_{\alpha=c,v} \beta_{\alpha\mathbf{q}}(t)\Phi^{(H)}_{\alpha\mathbf{q}}(\mathbf{r},t), \tag{5}$$

where $\beta_{\alpha\mathbf{q}}(t)$ are expansion coefficients.

Let us introduce the following quantities

$$\boldsymbol{\mathcal{A}}'_{\alpha'\alpha}(\mathbf{q},t) = \boldsymbol{\mathcal{A}}_{\alpha'\alpha}[\mathbf{k}(\mathbf{q},t)]\exp\left(i\phi^{(\mathrm{d})}_{\alpha'\alpha}(\mathbf{q},t)\right), \tag{6}$$

$$\phi^{(\mathrm{d})}_{\alpha'\alpha}(\mathbf{q},t) = \frac{1}{\hbar}\int_{-\infty}^{t} dt' \left(E_{\alpha'}[\mathbf{k}(\mathbf{q},t')] - E_\alpha[\mathbf{k}(\mathbf{q},t')]\right), \tag{7}$$

$$\boldsymbol{\mathcal{A}}_{\alpha'\alpha}(\mathbf{q}) = \left\langle \Psi^{(\alpha')}_{\mathbf{q}} \middle| i\frac{\partial \Psi^{(\alpha)}_{\mathbf{q}}}{\partial \mathbf{q}} \right\rangle, \mathbf{D}_{\alpha'\alpha}(\mathbf{q}) = e\boldsymbol{\mathcal{A}}_{\alpha'\alpha}(\mathbf{q}). \tag{8}$$

Here $\alpha, \alpha' = \mathrm{v}, \mathrm{c}_1, \mathrm{c}_2$ are band indices, $\alpha \neq \alpha'$; $\boldsymbol{\mathcal{A}}_{\alpha'\alpha}(\mathbf{q})$ is a matrix element of the non-Abelian Berry connection[54–56], $\mathbf{D}_{\alpha'\alpha}(\mathbf{q})$ the interband dipole matrix element, and $\phi^{(\mathrm{d})}_{\alpha'\alpha}(\mathbf{q},t)$ is the dynamic phase.

We introduce TDSE in the interaction representation in the adiabatic basis of the Houston functions as

$$i\hbar\frac{\partial B_{\mathbf{q}}(t)}{\partial t} = H'(\mathbf{q},t)B_{\mathbf{q}}(t) \ , \tag{9}$$

where wave function (vector of state) $B_{\mathbf{q}}(t)$ and Hamiltonian $H'(\mathbf{q},t)$ are defined as

$$B_{\mathbf{q}}(t) = \begin{bmatrix} \beta_{c_2\mathbf{q}}(t) \\ \beta_{c_1\mathbf{q}}(t) \\ \beta_{v\mathbf{q}}(t) \end{bmatrix} \ , \tag{10}$$

$$H'(\mathbf{q},t) = -e\mathbf{F}(t)\hat{\boldsymbol{\mathcal{A}}}(\mathbf{q},t) \ , \tag{11}$$

$$\hat{\boldsymbol{\mathcal{A}}}(\mathbf{q},t) = \begin{bmatrix} 0 & \boldsymbol{\mathcal{A}}'_{\mathrm{c_2c_1}}(\mathbf{q},t) & \boldsymbol{\mathcal{A}}'_{\mathrm{c_2v}}(\mathbf{q},t) \\ \boldsymbol{\mathcal{A}}'^{*}_{\mathrm{c_2c_1}}(\mathbf{q},t) & 0 & \boldsymbol{\mathcal{A}}'_{\mathrm{c_1v}}(\mathbf{q},t) \\ \boldsymbol{\mathcal{A}}'^{*}_{\mathrm{c_2v}}(\mathbf{q},t) & \boldsymbol{\mathcal{A}}'^{*}_{\mathrm{c_1v}}(\mathbf{q},t) & 0 \end{bmatrix}. \tag{12}$$

Matrix $\hat{\boldsymbol{\mathcal{A}}}(\mathbf{q},t)$ is the non-Abelian Berry connection in the interaction representation.

Schrödinger equation (9) defines dynamics of the system with accuracy limited by the truncation of the Hilbert space. Using Eq. (2), a general solution of Eq. (9) can be presented in terms of the evolution operator, $\hat{S}(\mathbf{q},t)$, as

$$B_{\mathbf{q}}(t) = \hat{S}(\mathbf{q},t)B_{\mathbf{q}}(-\infty) \ , \tag{13}$$

$$\hat{S}(\mathbf{q},t) = \hat{T}\exp\left[i\int_{t'=-\infty}^{t} \hat{\boldsymbol{\mathcal{A}}}(\mathbf{q},t')d\mathbf{k}(\mathbf{q},t')\right] \ , \tag{14}$$

where $\hat{T}$ is the time-ordering operator[57], and the integral is affected along Bloch trajectory $\mathbf{k}(\mathbf{q},t)$ [Eq. (2)].

We numerically solve TDSE (9) with initial conditions $\beta_{\mathrm{v}\mathbf{q}}(-\infty) = 1, \beta_{\mathrm{c}_1\mathbf{q}}(-\infty) = 0, \beta_{\mathrm{c}_2\mathbf{q}}(-\infty) = 0$. The total population of the CBs is $N_{\mathrm{CB}}(\mathbf{q},t) = \left|\beta_{\mathrm{c}_1\mathbf{q}}(t)\right|^2 + \left|\beta_{\mathrm{c}_2\mathbf{q}}(t)\right|^2$. After the pulse ends, there remains residual CB population $N^{(\mathrm{res})}_{\mathrm{CB}}(\mathbf{q}) = N_{\mathrm{CB}}(\mathbf{q},\infty)$.

The field of a single-oscillation right-hand circular-polarized pulse [see Eq. (1)] is displayed in Fig. 1(a) and the $\mathcal{T}$-reversed, left-hand pulse in Fig. 1(b). The residual CB population for MoS_2 induced by such a pulse with an amplitude of $F_0 = 0.25$ VÅ^{-1} is displayed in Figs. 1(c), (d) for spin-up ($s_z = 1/2$ or $\uparrow$) and Figs. 1(e), (f) for spin-down ($s_z = -1/2$ or $\downarrow$). Valley polarization is high: the right-handed pulse populates predominantly the K valleys, while the left-handed pulse excites mostly the K′ valleys. Protected by the $\mathcal{T}$-symmetry, the $\mathrm{K}_\uparrow$-valley population for a given handedness pulse is inversed ($\mathbf{k} \leftrightarrow -\mathbf{k}$) to the $\mathrm{K}'_\downarrow$-valley population for the opposite handedness; the same is true for $\mathrm{K}_\downarrow$ and $\mathrm{K}'_\uparrow$. Correspondingly, panel (c) is center-reflected to panel (f), and panel (d) to panel (e). The valley polarization is large, $\eta_{\mathrm{V}} \gtrsim 40\% - 60\%$ for at $F_0 = 0.1 - 0.25$ VÅ^{-1} – see Sec. VI of SM. There is also an appreciable, though smaller, spin polarization due to SOC.

We also performed computations for a two-oscillation pulse (see SM Fig. 3) and found no fundamental difference from the single-oscillation pulses. In fact, both the valley polarization and CB population become higher.

The valley and spin polarization in TMDC's caused by relatively weak (perturbative) circularly-polarized continuous-wave (CW) radiation[21,24,25] or relatively long 30 fs pulses[40] were previously known and attributed to angular momentum conservation at the

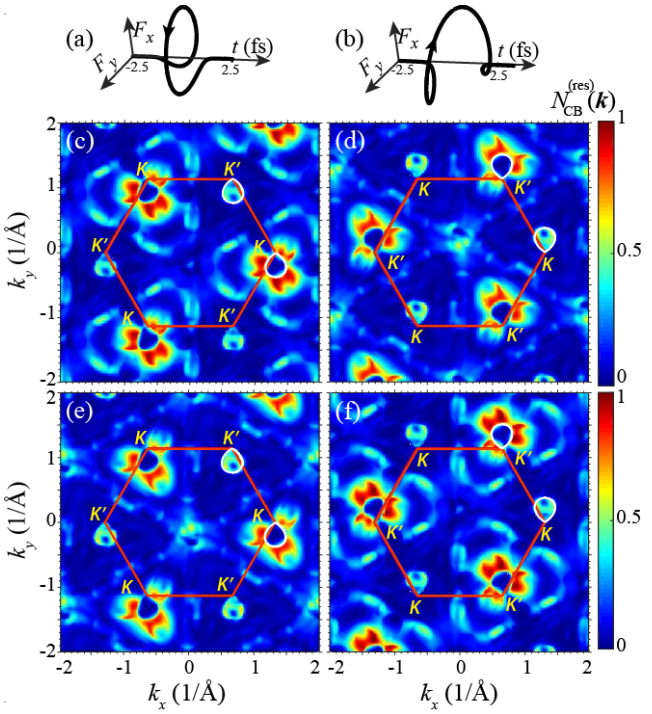

FIG. 1. Residual CB population $N^{(\mathrm{res})}_{\mathrm{CB}}(\mathbf{k})$ for monolayer MoS_2 in the extended zone picture. The red solid line shows the first Brillouin zone boundary with K, K'-points indicated. The amplitude of the optical field is $F_0 = 0.25$ VÅ^{-1}. (a) Waveform $\mathbf{F}(t)$ for right-handed circularly-polarized pulse. (b) The same as panel (a) but for left-handed circularly-polarized pulse [$\mathcal{T}$-reversed to that in panel (a)]. (c) Residual population of spin-up electrons, $N^{(\mathrm{res})}_{\mathrm{CB}\uparrow}(\mathbf{k})$, for right-handed pulse. (d) The same as (c), $N^{(\mathrm{res})}_{\mathrm{CB}\uparrow}(\mathbf{k})$, but for left-handed pulse. (e) Residual population of spin-down electrons, $N^{(\mathrm{res})}_{\mathrm{CB}\downarrow}(\mathbf{k})$, for right-handed pulse. (f) The same as (e), $N^{(\mathrm{res})}_{\mathrm{CB}\downarrow}(\mathbf{k})$, but for left-handed pulse.

K, K'-points[21,26]. The spin polarization is related to the intrinsic SOC in the transition metals[20,21,26].

A distinction of this work is that the significant CB population and valley polarization (along with a smaller spin polarization) can be written by a *single-oscillation* strong chiral pulse. The read-out can also be done by a single-oscillation chiral pulse: optical absorption of the read-out pulse of the same chirality will be reduced due to the Pauli blocking, while the opposite-chirality pulse absorption will not be attenuated because it interacts with the other, unpopulated valley. This one-optical-cycle recording and read-out make a basis of a fundamentally fastest optical memory.

Figures 2 (a) and (b) illustrates the residual CB population for another TMDC, WS_2, after a right-handed circularly polarized pulse with the amplitude of $F_0 = 0.25$ VÅ^{-1} for spin up and spin down electrons, respectively. Similar to Fig. 1, the right-handed single-oscillation pulse populates predominantly the K valleys. Due to stronger

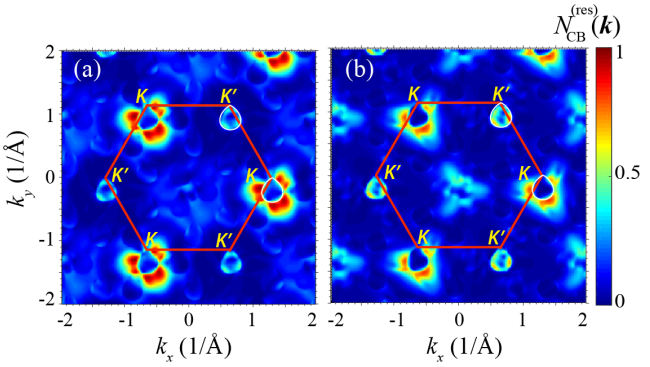

FIG. 2. Residual CB populations $N^{(\mathrm{res})}_{\mathrm{CB}}(\mathbf{k})$ for monolayer WS_2 after right-handed circularly polarized pulse. Note that the corresponding distributions for left-handed pulses are related to these by the $\mathcal{T}$-symmetry similar to Fig. 1. The red solid line shows the Brillouin zone boundary. Amplitude of the applied field is $F_0 = 0.25$ VÅ^{-1}. (a) Population $N^{(\mathrm{res})}_{\mathrm{CB}\downarrow}(\mathbf{k})$ for spin up electrons. (b) The same as panel (a) but for spin down electrons, $N^{(\mathrm{res})}_{\mathrm{CB}\uparrow}(\mathbf{k})$.

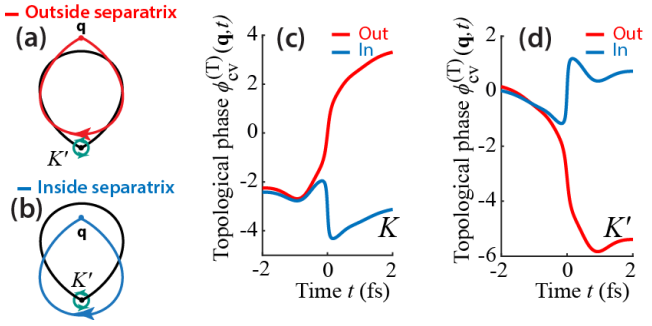

FIG. 3. For a chiral left-handed pulse, Bloch trajectories $\mathbf{k}(\mathbf{q},t)$ in the K' valley and topological phase $\phi^{(\mathrm{T})}_{\mathrm{cv}}(\mathbf{q},t)$ for transitions $v \to c$ between bands forming the bandgaps at the K- and K'-points. (a) Separatrix for the pulse used is shown by the black line. Electron Bloch trajectory $\mathbf{k}(\mathbf{q},t)$ is shown for initial point $\mathbf{q}$ outside the separatrix. The K'-point is denoted by a solid dot and the Berry connection is denoted by a green "whirl" where the chirality is indicated by arrows. (b) The same as (a) but for $\mathbf{q}$ inside the separatrix. (c) Topological phase $\phi^{(\mathrm{T})}_{\mathrm{cv}}(\mathbf{q},t)$ on the Bloch trajectory for the K-point and $\mathbf{q}$ outside of the separatrix (red line) and inside the separatrix (blue line). (d) The same as (c) but for the K' point.

SOC in W in comparison to Mo, the spin dependence is more pronounced.

The known valley selection rules for chiral pulses[21,23–27,58] are angular momentum perturbative selection rules, which are local in $\mathbf{k}$. In contrast, there is also fundamentally different, nonlinear-optical selection rule characteristic of strong-field excitation, which is evident from Figs. 1 and 2: In all cases when a given valley is favored by the angular momentum

selection rule, its population predominantly occurs *outside* of a closed curve (called separatrix[47]). This is the case for K-valleys in Figs. 1 (c), (e) and Fig. 2 and for the K'-valleys in Fig. 1 (d), (f). In the opposite case, when the angular momentum selection rule suppresses a valley's population, then the momentum states *inside* the separatrix are predominantly but weakly populated as is the case for the K'-valleys in Figs. 1 (c), (e) and Fig. 2 and the K-valleys in Figs. 1 (d), (f).

Formation of such textures is a fundamental effect, which is non-local in $\mathbf{k}$ and directly related to global topology of the Bloch bands. It is inherent in the strong-field excitation where an electron moves in the reciprocal space exploring the non-Abelian Berry connection, $\hat{\boldsymbol{\mathcal{A}}}(\mathbf{k})$, along its Bloch trajectory – cf. Eq. (14). We call it a *topological resonance*.

To understand the topological resonance, we turn to Figs. 3 (a), (b). The separatrix, which is shown by a closed black line, is defined as a set of initial points $\mathbf{q}$ for which electron trajectories pass precisely through the corresponding K or K' points[47]. Its parametric equation is $\mathbf{q}(t) = \mathbf{K} - \mathbf{k}(0,t)$, or $\mathbf{q}(t) = \mathbf{K}' - \mathbf{k}(0,t)$ where $t \in (-\infty, \infty)$ is a parameter. For initial crystal momentum $\mathbf{q}$ outside of the separatrix, the electron trajectory, $\mathbf{k}(\mathbf{q},t)$, does not encircle the K-point as in Fig. 3 (a), otherwise it does as in Fig. 3 (b).

Evolution operator of Eq. (14) describes a deeply nonlinear, complex quantum dynamics of the photo-excitation whose exact evaluation can only be done numerically, cf. Figs. (1) and (2) above. To get a qualitative insight, consider Eq. (14) in the first order of perturbation theory, where it becomes

$$\hat{S}(\mathbf{q},t) = 1 + i\int_{t'=-\infty}^{t} \hat{\boldsymbol{\mathcal{A}}}(\mathbf{q},t')d\mathbf{k}(\mathbf{q},t') \ . \qquad (15)$$

Correspondingly, residual (after the pulse ends) CB population n_α is

$$n_\alpha = \left| \oint \left| \boldsymbol{\mathcal{A}}_{\alpha\mathrm{v}}[\mathbf{k}(\mathbf{q},t)]\mathbf{n}(t) \right| \times \right.$$
$$\left. \exp\left[i\phi^{(\mathrm{tot})}_{\alpha\mathrm{v}}(\mathbf{q},t) \right] dk(\mathbf{q},t) \right|^2 , \qquad (16)$$

where $\alpha = c_1, c_2$, and the integral is affected along a closed-loop Bloch trajectory (2) whose parametric form is $\mathbf{k}(\mathbf{q},t)$ with parameter $t \in \{-\infty, \infty\}$, $\mathbf{n}(t) = \mathbf{F}(t)/F(t)$ is unit vector tangential to the Bloch trajectory, total phase $\phi^{(\mathrm{tot})}$ is expressed as

$$\phi^{(\mathrm{tot})}_{\alpha v} = \phi^{(\mathrm{T})}_{\alpha\mathrm{v}}(\mathbf{q},t) + \phi^{(\mathrm{d})}_{\alpha\mathrm{v}}(\mathbf{q},t) \ , \qquad (17)$$

and topological phase is defined as

$$\phi^{(\mathrm{T})}_{\alpha\mathrm{v}}(\mathbf{q},t) = \arg\left\{ \boldsymbol{\mathcal{A}}_{\alpha\mathrm{v}}[\mathbf{k}(\mathbf{q},t)]\mathbf{n}(t) \right\} \ . \qquad (18)$$

Note that the non-Abelian Berry connection element, $\boldsymbol{\mathcal{A}}_{\alpha\mathrm{v}}[\mathbf{k}(\mathbf{q},t)]$, and the topological phase, $\phi^{(\mathrm{T})}_{\alpha\mathrm{v}}(\mathbf{q},t)$, are not gauge-invariant, and, correspondingly, are not observable. However, the CB population, n_α, as given by a closed-loop integral of Eq. (16), is observable. Also, the total change of the topological phase during the pulse, $\Delta\phi^{(\mathrm{T})}_{\alpha\mathrm{v}}(\mathbf{q}) = \phi^{(\mathrm{T})}_{\alpha\mathrm{v}}(\mathbf{q},\infty) - \phi^{(\mathrm{T})}_{\alpha\mathrm{v}}(\mathbf{q},-\infty)$, can be observed interferometrically in a two-cycle experiment as proposed earlier[47]. It is, therefore, also gauge invariant.

The topological phase, $\phi^{(\mathrm{T})}_{\alpha\mathrm{v}}(\mathbf{q},t)$ (18), is displayed in Fig. 3 (c) for the K-valley and in Fig. 3 (d) for the K'-valley. The total changes of this phase for the valleys with opposite chiralities are opposite, as protected by the $\mathcal{T}$-symmetry. For initial crystal momentum $\mathbf{q}$ outside of the separatrix, this change is significantly larger in magnitude than otherwise (cf. the red vs. blue lines) and is close to $\pm 2\pi$.

In Eq. (16), modulus $\left|\boldsymbol{\mathcal{A}}_{\alpha\mathrm{v}}[\mathbf{k}(\mathbf{q},t)]\mathbf{n}(t)\right|$ is a smooth function of time; it is the oscillating phase factor, $\exp\left[i\phi^{(\mathrm{tot})}_{\alpha\mathrm{v}}(\mathbf{q},t)\right]$ that determines whether the integral is large or small. If the topological phase, $\phi^{(\mathrm{T})}_{\alpha\mathrm{v}}(\mathbf{q},t)$, and the dynamic phase, $\phi^{(\mathrm{d})}_{\alpha\mathrm{v}}(\mathbf{q},t)$, mutually cancel each other in Eq. (17), then the accumulation along the Bloch trajectory in the integral of Eq. (16) is coherent, and n_α is large. If to the opposite, the dynamic phase and topological phase add to each other, then the phase exponential in Eq. (16) oscillates more rapidly, and the contributions along the Bloch trajectory tend to mutually cancel each other leading to a small value of n_α.

Under resonant conditions, dynamic phase $\phi^{(\mathrm{d})}_{\mathrm{cv}}(\mathbf{q},t)$ [Eq. (7)] during the pulse monotonically increases with time t by $\approx 2\pi$. Hence, the topological resonance takes place for the topological phase, $\phi^{(\mathrm{T})}_{\mathrm{cv}}(\mathbf{q},t)$, decreasing by the same amount, $\Delta\phi^{(\mathrm{T})}_{\mathrm{cv}} \approx -2\pi$. For the case of a left-handed pulse illustrated in Fig. 3, this topological resonance occurs for crystal momentum $\mathbf{q}$ outside of the separatrix for the K'-point [see the red curve in Fig. 3(d)].

For the same example of a left-handed pulse illustrated in Fig. 3, if $\mathbf{q}$ is inside the separatrix, then the change of the topological phase during the pulse for the K-point is $\Delta\phi^{(\mathrm{T})}_{\mathrm{cv}} \approx -\pi$. In such a case, there is only a partial phase compensation. This leads to a weak population of the K-valley inside the separatrix. This qualitative picture is precisely what one can see in Figs. 1 (d) and (f): a strong population of the K'-valley outside of the separatrix and a weak population of the K-valley inside the separatrix. Note that the topological resonance only weakly depends on spin [panels (d) and (f) are very similar], because the SOC is still relatively weak. Protected by the $\mathcal{T}$-reversal symmetry, for the opposite chirality of the pulse, the K- and K'-valleys are exchanged, and the spin is changed to the opposite – cf. Figs. 1 (d), (f) with Figs. 1 (c), (e). These properties of the topological resonance are general for all TMDC's: cf. Figs. 1 (c), (e) with Figs. 2 (a), (b).

To conclude, we have demonstrated a fundamental possibility to induce a significant CB populations and valley polarization in TMDC's during just one optical period of a chiral, moderately-high field ($F_0 \sim 0.25$ V/Å) laser pulse. This is a wide-band ultrafast process which is defined by the topological resonance that we have in-

troduced above in this article. This resonance is due to mutual compensation of the dynamic phase and the non-Abelian Berry phase, which brings about formation of textures in the **k**-space with discontinuities at the separatrices. These textures can be directly observed using the time-resolved angle-resolved photoelectron spectroscopy[59].

The topological resonances can be present and pronounced not only in TMDC's but also in other materials with direct bandgap at the Brillouin zone boundary, e.g., hexagonal boron nitride et al.[60]. The topological resonances can also be present in materials where the direct bandgap is not at one of the $\mathcal{T}$-invariant points such as the Γ-point or the M-points. The presence of the bandgap is essential because it causes a gradual accumulation of the non-Abelian Berry phase along the Bloch **k**-space electron trajectory, which is necessary to compensate the gradually accumulating dynamic phase.

The predicted induction of the valley polarization promises a wide range of important valleytronics applications, in particular, to PHz-band information processing and storage. The predicted topological resonance is a new concept, which will stimulate novel developments in topological strong-field optics of solids. In particular, the chiral, non-uniform electron distributions in the reciprocal space will cause chiral currents in the real space, which we will consider elsewhere.

ACKNOWLEDGMENTS

Major funding was provided by Grant No. DE-FG02-01ER15213 from the Chemical Sciences, Biosciences and Geosciences Division, Office of Basic Energy Sciences, Office of Science, US Department of Energy. Numerical simulations have been performed using support by Grant No. DE-FG02-11ER46789 from the Materials Sciences and Engineering Division of the Office of the Basic Energy Sciences, Office of Science, U.S. Department of Energy. The work of V.A. was supported by Grant No. ECCS-1308473 from NSF. Support for S.A.O.M. came from a MURI Grant No. FA9550-15-1-0037 from the US Air Force of Scientific Research, and for J.-S.W. from a NSF EFRI NewLAW Grant EFMA-17 41691.

[1] Hanieh Fattahi, Helena G. Barros, Martin Gorjan, Thomas Nubbemeyer, Bidoor Alsaif, Catherine Y. Teisset, Marcel Schultze, Stephan Prinz, Matthias Haefner, Moritz Ueffing, Ayman Alismail, Lenard Vamos, Alexander Schwarz, Oleg Pronin, Jonathan Brons, Xiao Tao Geng, Gunnar Arisholm, Marcelo Ciappina, Vladislav S. Yakovlev, Dong-Eon Kim, Abdallah M. Azzeer, Nicholas Karpowicz, Dirk Sutter, Zsuzsanna Major, Thomas Metzger, and Ferenc Krausz, "Third-generation femtosecond technology," Optica **1**, 45–63 (2014).

[2] A. Schiffrin, T. Paasch-Colberg, N. Karpowicz, V. Apalkov, D. Gerster, S. Muhlbrandt, M. Korbman, J. Reichert, M. Schultze, S. Holzner, J. V. Barth, R. Kienberger, R. Ernstorfer, V. S. Yakovlev, M. I. Stockman, and F. Krausz, "Optical-field-induced current in dielectrics," Nature **493**, 70–74 (2012).

[3] M. Schultze, E. M. Bothschafter, A. Sommer, S. Holzner, W. Schweinberger, M. Fiess, M. Hofstetter, R. Kienberger, V. Apalkov, V. S. Yakovlev, M. I. Stockman, and F. Krausz, "Controlling dielectrics with the electric field of light," Nature **493**, 75–8 (2013).

[4] A. V. Mitrofanov, A. J. Verhoef, E. E. Serebryannikov, J. Lumeau, L. Glebov, A. M. Zheltikov, and A. Baltuška, "Optical detection of attosecond ionization induced by a few-cycle laser field in a transparent dielectric material," Phys. Rev. Lett. **106**, 147401–1–4 (2011).

[5] E. Goulielmakis, V. S. Yakovlev, A. L. Cavalieri, M. Uiberacker, V. Pervak, A. Apolonski, R. Kienberger, U. Kleineberg, and F. Krausz, "Attosecond control and measurement: Lightwave electronics," Science **317**, 769–775 (2007).

[6] T. Paasch-Colberg, S. Y. Kruchinin, O. Saglam, S. Kapser, S. Cabrini, S. Muehlbrandt, J. Reichert, J. V. Barth, R. Ernstorfer, R. Kienberger, V. S. Yakovlev, N. Karpowicz, and A. Schiffrin, "Sub-cycle optical control of current in a semiconductor: from the multiphoton to the tunneling regime," Optica **3**, 1358–1361 (2016).

[7] Q. H. Wang, K. Kalantar-Zadeh, A. Kis, J. N. Coleman, and M. S. Strano, "Electronics and optoelectronics of two-dimensional transition metal dichalcogenides," Nature Nanotechnology **7**, 699–712 (2012).

[8] L. Britnell, R. M. Ribeiro, A. Eckmann, R. Jalil, B. D. Belle, A. Mishchenko, Y. J. Kim, R. V. Gorbachev, T. Georgiou, S. V. Morozov, A. N. Grigorenko, A. K. Geim, C. Casiraghi, A. H. C. Neto, and K. S. Novoselov, "Strong light-matter interactions in heterostructures of atomically thin films," Science **340**, 1311–1314 (2013).

[9] F. Withers, O. Del Pozo-Zamudio, A. Mishchenko, A. P. Rooney, A. Gholinia, K. Watanabe, T. Taniguchi, S. J. Haigh, A. K. Geim, A. I. Tartakovskii, and K. S. Novoselov, "Light-emitting diodes by band-structure engineering in van der Waals heterostructures," Nat. Mater. **14**, 301–306 (2015).

[10] G. B. Liu, D. Xiao, Y. G. Yao, X. D. Xu, and W. Yao, "Electronic structures and theoretical modelling of two-dimensional group-VIB transition metal dichalcogenides," Chem. Soc. Rev. **44**, 2643–2663 (2015).

[11] K. S. Novoselov, A. Mishchenko, A. Carvalho, and A. H. C. Neto, "2d materials and van der Waals heterostructures," Science **353**, 461–1–11 (2016).

[12] Y. Ye, J. Xiao, H. L. Wang, Z. L. Ye, H. Y. Zhu, M. Zhao, Y. Wang, J. H. Zhao, X. B. Yin, and X. Zhang, "Electrical generation and control of the valley carriers in a monolayer transition metal dichalcogenide," Nature Nanotechnology **11**, 598–602 (2016).

[13] H. Z. Liu, Y. L. Li, Y. S. You, S. Ghimire, T. F. Heinz, and D. A. Reis, "High-harmonic generation from an atomically thin semiconductor," Nat. Phys. **13**, 262–266 (2017).

[14] M. Ashton, J. Paul, S. B. Sinnott, and R. G. Hennig, "Topology-scaling identification of layered solids and stable exfoliated 2d materials," Phys. Rev. Lett. **118** (2017).

[15] Max C. Lemme, Lain-Jong Li, Toms Palacios, and Frank Schwierz, "Two-dimensional materials for electronic applications," MRS Bulletin **39**, 711718 (2014).

[16] K. S. Novoselov, V. I. Falko, L. Colombo, P. R. Gellert, M. G. Schwab, and K. Kim, "A roadmap for graphene," Nature **490**, 192–200 (2012).

[17] D. Jariwala, V. K. Sangwan, L. J. Lauhon, T. J. Marks, and M. C. Hersam, "Emerging device applications for semiconducting two-dimensional transition metal dichalcogenides," Acs Nano **8**, 1102–1120 (2014).

[18] A. K. Geim and K. S. Novoselov, "The rise of graphene," Nat Mater **6**, 183–191 (2007).

[19] F. Schwierz, "Graphene transistors," Nature Nanotechnology **5**, 487–496 (2010).

[20] G. B. Liu, W. Y. Shan, Y. G. Yao, W. Yao, and D. Xiao, "Three-band tight-binding model for monolayers of group-VIB transition metal dichalcogenides," Phys. Rev. B **88**, 085433–1–10 (2013).

[21] D. Xiao, G. B. Liu, W. X. Feng, X. D. Xu, and W. Yao, "Coupled spin and valley physics in monolayers of MoS_2 and other group-VI dichalcogenides," Phys. Rev. Lett. **108** (2012).

[22] J. W. Jiang, "Graphene versus MoS_2: A short review," Frontiers of Physics **10**, 287–302 (2015).

[23] E. J. Sie, J. McIver, Y. H. Lee, L. Fu, J. Kong, and N. Gedik, "Valley-selective optical stark effect in monolayer WS_2," Nature Materials **14**, 290–294 (2015).

[24] H. L. Zeng, J. F. Dai, W. Yao, D. Xiao, and X. D. Cui, "Valley polarization in MoS_2 monolayers by optical pumping," Nature Nanotechnology **7**, 490–493 (2012).

[25] K. F. Mak, K. L. He, J. Shan, and T. F. Heinz, "Control of valley polarization in monolayer MoS_2 by optical helicity," Nature Nanotechnology **7**, 494–498 (2012).

[26] T. Cao, G. Wang, W. P. Han, H. Q. Ye, C. R. Zhu, J. R. Shi, Q. Niu, P. H. Tan, E. Wang, B. L. Liu, and J. Feng, "Valley-selective circular dichroism of monolayer molybdenum disulphide," Nat. Commun. **3**, 887–1–5 (2012).

[27] A. M. Jones, H. Y. Yu, N. J. Ghimire, S. F. Wu, G. Aivazian, J. S. Ross, B. Zhao, J. Q. Yan, D. G. Mandrus, D. Xiao, W. Yao, and X. D. Xu, "Optical generation of excitonic valley coherence in monolayer WSe_2," Nature Nanotechnology **8**, 634–638 (2013).

[28] M. Eginligil, B. C. Cao, Z. L. Wang, X. N. Shen, C. X. Cong, J. Z. Shang, C. Soci, and T. Yu, "Dichroic spin-valley photocurrent in monolayer molybdenum disulphide," Nature Communications **6** (2015).

[29] M. Garg, M. Zhan, T. T. Luu, H. Lakhotia, T. Klostermann, A. Guggenmos, and E. Goulielmakis, "Multi-petahertz electronic metrology," Nature **538**, 359–363 (2016).

[30] P. Krogen, H. Suchowski, H. Liang, N. Flemens, K.-H. Hong, F. X. Kaertner, and J. Moses, "Generation and multi-octave shaping of mid-infrared intense single-cycle pulses," Nat. Phot. **11**, 222–227 (2017).

[31] H. Liang, P. Krogen, Z. Wang, H. Park, T. Kroh, K. Zawilski, P. Schunemann, J. Moses, L. F. DiMauro, F. X. Kaertner, and K.-H. Hong, "High-energy mid-infrared sub-cycle pulse synthesis from a parametric amplifier," Nat. Commun. **8**, 141–1–9 (2017).

[32] U. Elu, M. Baudisch, H. Pires, F. Tani, M. H. Frosz, F. Koettig, A. Ermolov, P. St.J. Russell, and J. Biegert, "High average power and single-cycle pulses from a mid-ir optical parametric chirped pulse amplifier," Optica **4**, 1024–1029 (2017).

[33] C. Vicario, M. Shalaby, and C. P. Hauri, "Subcycle extreme nonlinearities in gap induced by an ultrastrong terahertz field," Phys. Rev. Lett. **118**, 083901–1–5 (2017).

[34] S. S. Dhillon, M. S. Vitiello, E. H. Linfield, A. G. Davies, M. C. Hoffmann, J. Booske, C. Paoloni, M. Gensch, P. Weightman, G. P. Williams, E. Castro-Camus, D. R. S. Cumming, F. Simoens, I. Escorcia-Carranza, J. Grant, S. Lucyszyn, M. Kuwata-Gonokami, K. Konishi, M. Koch, C. A. Schmuttenmaer, T. L. Cocker, R. Huber, A. G. Markelz, Z. D. Taylor, V. P. Wallace, J. A. Zeitler, J. Sibik, T. M. Korter, B. Ellison, S. Rea, P. Goldsmith, K. B. Cooper, R. Appleby, D. Pardo, P. G. Huggard, V. Krozer, H. Shams, M. Fice, C. Renaud, A. Seeds, A. Stohr, M. Naftaly, N. Ridler, R. Clarke, J. E. Cunningham, and M. B. Johnston, "The 2017 terahertz science and technology roadmap," J. Phys. D Appl. Phys. **50**, 043001–1–49 (2017).

[35] F. Langer, M. Hohenleutner, U. Huttner, S. W. Koch, M. Kira, and R. Huber, "Symmetry-controlled temporal structure of high-harmonic carrier fields from a bulk crystal," Nat. Phot. **11**, 227–231 (2017).

[36] J. Li, X. Ren, Y. Yin, Y. Cheng, E. Cunningham, Y. Wu, and Z. Chang, "Polarization gating of high harmonic generation in the water window," Appl. Phys. Lett. **108**, 231102–1–5 (2016).

[37] S. Sim, J. Park, J. G. Song, C. In, Y. S. Lee, H. Kim, and H. Choi, "Exciton dynamics in atomically thin MoS_2: Interexcitonic interaction and broadening kinetics," Phys. Rev. B **88** (2013).

[38] G. Moody, J. Schaibley, and X. D. Xu, "Exciton dynamics in monolayer transition metal dichalcogenides," Journal of the Optical Society of America B-Optical Physics **33**, C39–C49 (2016).

[39] Z. G. Nie, R. Long, L. F. Sun, C. C. Huang, J. Zhang, Q. H. Xiong, D. W. Hewak, Z. X. Shen, O. V. Prezhdo, and Z. H. Loh, "Ultrafast carrier thermalization and cooling dynamics in few-layer MoS_2," Acs Nano **8**, 10931–10940 (2014).

[40] Y.-T. Wang, C.-W. Luo, A. Yabushita, K.-H. Wu, T. Kobayashi, C.-H. Chen, and L.-J. Li, "Ultrafast multi-level logic gates with spin-valley coupled polarization anisotropy in monolayer MoS_2," Sci. Rep. **5**, 8289–1–6 (2015).

[41] V. Apalkov and M. I. Stockman, "Theory of dielectric nanofilms in strong ultrafast optical fields," Phys. Rev. B **86**, 165118–1–13 (2012).

[42] V. Apalkov and M. I. Stockman, "Metal nanofilm in strong ultrafast optical fields," Phys. Rev. B **88**, 245438–1–7 (2013).

[43] T. Higuchi, M. I. Stockman, and P. Hommelhoff, "Strong-field perspective on high-harmonic radiation from bulk solids," Phys. Rev. Lett. **113**, 213901–1–5 (2014).

[44] H. K. Kelardeh, V. Apalkov, and M. I. Stockman, "Wannier-stark states of graphene in strong electric field," Phys. Rev. B **90**, 085313–1–11 (2014).

[45] H. K. Kelardeh, V. Apalkov, and M. I. Stockman, "Graphene in ultrafast and superstrong laser fields," Phys. Rev. B **91**, 0454391–8 (2015).

[46] H. K. Kelardeh, V. Apalkov, and M. I. Stockman, "Ultrafast field control of symmetry, reciprocity, and reversibility in buckled graphene-like materials," Phys. Rev. B **92**, 045413–1–9 (2015).

[47] H. K. Kelardeh, V. Apalkov, and M. I. Stockman, "Attosecond strong-field interferometry in graphene: Chirality, singularity, and Berry phase," Phys. Rev. B **93**, 155434–1–7 (2016).

[48] M. S. Wismer, S. Y. Kruchinin, M. Ciappina, M. I. Stockman, and V. S. Yakovlev, "Strong-field resonant dynamics in semiconductors," Phys. Rev. Lett. **116**, 197401–1–5 (2016).

[49] S. A. Oliaei Motlagh, V. Apalkov, and M. I. Stockman, "Interaction of crystalline topological insulator with an ultrashort laser pulse," Phys. Rev. B **95**, 085438–1–8 (2017).

[50] O. Kwon, T. Paasch-Colberg, V. Apalkov, B.-K. Kim, J.-J. Kim, M. I. Stockman, and D. E. Kim, "Semimetallization of dielectrics in strong optical fields," Sci. Rep. **6**, 21272–1–9 (2016).

[51] T. Higuchi, C. Heide, K. Ullmann, H. B. Weber, and P. Hommelhoff, "Light-field-driven currents in graphene," Nature **550**, 224–228 (2017).

[52] F. Bloch, "Über die Quantenmechanik der Elektronen in Kristallgittern," Z. Phys. A **52**, 555–600 (1929).

[53] W. V. Houston, "Acceleration of electrons in a crystal lattice," Phys. Rev. **57**, 184–186 (1940).

[54] F. Wilczek and A. Zee, "Appearance of gauge structure in simple dynamical systems," Phys. Rev. Lett. **52**, 2111–2114 (1984).

[55] D. Xiao, M.-C. Chang, and Q. Niu, "Berry phase effects on electronic properties," Rev. Mod. Phys. **82**, 1959–2007 (2010).

[56] F. Yang and R. B. Liu, "Nonlinear optical response induced by non-Abelian Berry curvature in time-reversal-invariant insulators," Phys. Rev. B **90**, 245205 (2014).

[57] A. A. Abrikosov, L. P. Gorkov, and I. E. Dzi aloshinskii, *Methods of Quantum Field Theory in Statistical Physics* (Dover Publications, New York, 1975).

[58] W. Yao, D. Xiao, and Q. Niu, "Valley-dependent optoelectronics from inversion symmetry breaking," Phys. Rev. B **77**, 235406–1–7 (2008).

[59] Y. Liu, G. Bian, T. Miller, and T. C. Chiang, "Visualizing electronic chirality and Berry phases in graphene systems using photoemission with circularly polarized light," Phys. Rev. Lett. **107**, 166803–1–5 (2011).

[60] M. S. Xu, T. Liang, M. M. Shi, and H. Z. Chen, "Graphene-like two-dimensional materials," Chem. Rev. **113**, 3766–3798 (2013).